nature communications

Article

https://doi.org/10.1038/s41467-024-54435-3

Acid-exposed and hypoxic cancer cells do not overlap but are interdependent for unsaturated fatty acid resources

Received: 13 March 2024

Accepted: 7 November 2024

Published online: 21 November 2024

Check for updates

Katarzyna Głowacka[1,8], Sébastien Ibanez[1,8], Ophélie Renoult[1], Perrine Vermonden[2], Maria Virginia Giolito[1], Kübra Özkan[1], Charline Degavre[1], Léo Aubert[1], Céline Guilbaud[1], Florine Laloux-Morris[1], Elena Richiardone[1], Jérôme Ambroise[3], Caroline Bouzin[4], Davide Brusa[5], Jonas Dehairs[6], Johan Swinnen[6], Cyril Corbet[1], Yvan Larondelle[2] & Olivier Feron[1,7]

Cancer cells in acidic tumor regions are aggressive and a key therapeutic target, but distinguishing between acid-exposed and hypoxic cells is challenging. Here, we use carbonic anhydrase 9 (CA9) antibodies to mark acidic areas in both hypoxic and respiring tumor areas, along with an HRE-GFP reporter for hypoxia, to isolate distinct cell populations from 3D tumor spheroids. Transcriptomic analysis of CA9-positive, hypoxia-negative cells highlights enriched fatty acid desaturase activity. Inhibiting or silencing stearoyl-CoA desaturase-1 (SCD1) induces ferroptosis in CA9-positive acidic cancer cells and delays mouse tumor growth, an effect enhanced by omega-3 fatty acid supplementation. Using acid-exposed cancer cells and patient-derived tumor organoids, we show that SCD1 inhibition increases acidic cancer cell reliance on external mono-unsaturated fatty acids, depriving hypoxic cells of essential resources. This bystander effect provides unbiased evidence for a lack of full overlap between hypoxic and acidic tumor compartments, highlighting a rationale for targeting desaturase activity in cancer.

Tumor acidosis primarily results from a compromised capillary perfusion incapable of carrying away H^+ released (together with lactate) by hypoxic, glycolytic cancer cells[1,2]. While this statement might suggest a necessary association between acidosis and hypoxia, the interplay between these two cancer hallmarks is more complex. First, the preferred glucose fermentation into lactate together with two H^+ equivalents can occur in non-hypoxic tumor areas, a phenomenon initially described by Otto Warburg[3]. Second, glycolysis-impaired or lactate dehydrogenase-deficient cancer cells retain the ability to acidify the extracellular environment in vivo[4–6]. Third, a high respiratory rate of cancer cells may directly contribute to acidosis upon CO_2 generation and hydration in the extracellular medium ($CO_2 + H_2O \rightarrow HCO_3^- + H^+$)[7]. Acidosis may thus develop in tumor areas where O_2 is available but with a limited capacity to rapidly get rid of extracellular H^+. This claim is further supported by various sets of experimental data documenting a non-overlapping relationship between extracellular pH (pH_e) and pO_2[8,9]. A model may thus be proposed where, besides hypoxic (acidic) cancer cells located at a distance from blood vessels,

[1]Pole of Pharmacology and Therapeutics (FATH), Institut de Recherche Expérimentale et Clinique (IREC), UCLouvain, Brussels, Belgium. [2]Louvain Institute of Biomolecular Science and Technology (LIBST), UCLouvain, Louvain-la-Neuve, Belgium. [3]Centre des Technologies Moléculaires Appliquées (CTMA), Institut de Recherche Expérimentale et Clinique (IREC), UCLouvain, Brussels, Belgium. [4]Imaging Platform 2IP, Institut de Recherche Expérimentale et Clinique (IREC), UCLouvain, Brussels, Belgium. [5]CytoFlux-Flow Cytometry and Cell Sorting Platform, Institut de Recherche Expérimentale et Clinique (IREC), UCLouvain, Brussels, Belgium. [6]Laboratory of Lipid Metabolism and Cancer, Department of Oncology, KU Leuven and Leuven Cancer Institute (LKI), Leuven, Belgium. [7]Walloon Excellence in Life Sciences and BIOtechnology (WELBIO) Department, WEL Research Institute, Wavre, Belgium. [8]These authors contributed equally: Katarzyna Głowacka, Sébastien Ibanez. e-mail: olivier.feron@uclouvain.be

and well-perfused cancer cells bathing in a well-buffered extracellular medium, a third intermediary tumor compartment is made of non-hypoxic, acidic cancer cells[1]; non-hypoxic being understood in its large acceptance, i.e. moderately oxygenated.

We previously reported a shift from glycolysis to fatty acid metabolism in cancer cells of distinct origins chronically exposed to an acidic pH_e (*vs*. corresponding cancer cells maintained at physiological pH_e)[10]. Our lab further documented that acidic cancer cells could be concomitantly engaged in FA synthesis and oxidation[11]. More recently, a genome-wide CRISPR-Cas9 approach aiming to identify critical survival pathways for acidic cancer cells strengthened these findings with the identification of genes the expression of which supports mitochondrial respiration[12]. These data are also in line with the well-known inhibition of glycolytic enzymes in response to pH_i reduction and fit the recently reported enhanced PPAR pathway in acid-resistant cancer cells[13]. The search for such distinct pathways to therapeutically target acidic, non-hypoxic cancer cells gains particular relevance when contemplating the phenotype associated with this tumor compartment. Indeed, while acidosis is often associated with a reduction in cell proliferation[14], acidic cancer cells undergo an epithelial-to-mesenchymal phenotype under the control of different actors including TGFβ2[15] and RhoA[16] signaling, making them more prone to invasiveness and metastatic spreading. Rohani and colleagues also documented that tumor acidosis areas (not restricted to hypoxic regions) overlie highly proliferative and invasive zones at the tumor–stroma interface[17]. Targeting this tumor's acidic compartment thus represents an attractive strategy to kill cancer cells among the most aggressive tumors.

In this study, we, therefore, aimed to follow an unbiased strategy to isolate acidic, non-hypoxic cancer cells and profile them to formally prove the existence of this tumor compartment and identify potential vulnerabilities to target it. The challenge was to discriminate this cell population from the hypoxic cancer cells. To dissociate acidic from non-acidic cancer cells regardless of the hypoxic environment, we considered the double role of carbonic anhydrase CA9 with its extracellular-facing catalytic sites. Indeed, in a hypoxic area where reduction in intracellular pH (pH_i) requires dynamic export of H^+ (together with lactate) in the extracellular medium, CA9 facilitates consecutive extracellular H^+ diffusion upon enzymatic CO_2 formation (accelerating the otherwise slow spontaneous reaction kinetics: $H^+ + HCO_3^- \rightarrow H_2O + CO_2$). Interestingly, Swietach and colleagues documented that in the presence of environmental CO_2, CA9 activity could instead reduce pH_e by converting respiration-derived CO_2 to extracellular H^+[18,19]. These data aligned with the documented lack of correlation between CA9 expression and various hypoxia markers[20–22]. CA9 expression has thus the potential to act as a marker of acidosis not only in deeply hypoxic tumor regions but also in tumor areas where respiration supports cancer cell oxidative metabolism (and the associated reduction in pO_2 reaching a threshold compatible with CA9 expression). Combination with bona fide hypoxia markers could then offer discriminating tools to further isolate acidic cancer cells engaged in oxidative metabolism from hypoxic, glycolytic cancer cells. To maximize the tractability of this approach, we used 3D tumor spheroids where all the cells located at the same distance of the center share the same phenotype, making the different compartments mentioned above more defined. FACSorting of CA9-positive but deep hypoxia-negative cancer cells led us to identify desaturase SCD1 as a druggable vulnerability of acidic cancer cells, as further validated in mouse tumor models and patient-derived tumor organoids. This work also uncovered a symbiotic interplay between hypoxic and acidic cancer cells, the former being addicted to exogenous mono-unsaturated FA spared by SCD1-expressing cancer cells under acidosis, further reinforcing the rationale of targeting desaturase activity in cancer.

Results

CA9 expression does not strictly overlap with hypoxia markers

We first compared the extent of CA9-positive staining with the hypoxic area within 3D tumor spheroids. To detect hypoxia, we used either pimonidazole staining of spheroid slices (Fig. 1a) or the detection of GFP under the regulation of hypoxia-responsive elements (HREs) in sections of cleared spheroids using light sheet microscopy (Fig. 1b). The CA9-positive area was significantly larger than the hypoxic zone in 3D tumor spheroids generated from head and neck FaDu and colorectal HCT116 cancer cells (see bar graphs in Fig. 1a, b), indicating the presence of a CA9-positive (acidic) compartment that is not hypoxic or more exactly with a pO_2 above the threshold of pimonidazole and HRE-GFP detection; similar results were obtained with colorectal HT-29 spheroids (Fig. S1a). 3D imaging reconstruction of the whole spheroids (imaged by light sheet microscopy) confirmed that hypoxic and non-(or less) hypoxic CA9-positive compartments could be discriminated (Fig. 1c, see also Supplementary Movie 1). Mouse tumors generated from FaDu and HCT116 cancer cells also revealed that some CA9-positive areas did not overlap with pimonidazole-positive (hypoxic) areas (Fig. 1d); a differential CA9 and pimonidazole staining was also observed in HT-29 colorectal tumors (Fig. S1b). Finally, we examined by flow cytometry the level of CA9 expression in cancer cells adapted to pH 6.5 and corresponding cancer cells maintained at pH 7.4 (named 6.5/ and 7.4/cancer cells here below, respectively), both cell populations being cultured under oxygenated conditions. We found a net increase in CA9 expression in acid-exposed cancer cells (Figs. 1e and S1c, d), further validating CA9 as a marker to help track the acidic, oxidative tumor compartment.

CA9-positive HRE-negative cancer cells exhibit enrichment in FA desaturase activity

Next, we aimed to characterize the transcriptome of acidic, non-hypoxic cancer cells (as defined above) sorted from 3D spheroids using a combination of CA9 and HRE-GFP labeling (Fig. 2a). Four distinct cell populations isolated by FACS (Figs. 2b and S2a) were submitted to RNA-seq analysis. The principal component analysis confirmed significant differences between the 4 quadrants (Fig. 2c). As a validation, Gene Set Enrichment Analysis (GSEA) revealed that hypoxia and glycolysis pathways were enriched in double positive CA9+/HRE+ cell population, i.e. the bona fide hypoxic, glycolytic cell compartment (Fig. S2b). When compared with double positive CA9+/HRE+ cell population, CA9+/HRE- (i.e., acidic, non-hypoxic) cancer cells exhibited 1303 DE genes (FDR < 0.05) (Fig. 2d). KEGG analysis identified *ferroptosis* among the pathways enriched in CA9+/HRE− cells (Fig. 2e) further validating our sorting strategy. We have indeed documented that acidic cancer cells exhibit an increased susceptibility to lipid peroxidation and associated ferroptosis[23]. Interestingly, the top enriched pathway, i.e., *the biosynthesis of mono-unsaturated fatty acid (MUFA)* (Fig. 2e), could also be related to ferroptosis since MUFA are known to protect cells from ferroptosis[24,25]. In this MUFA synthesis-related pathway, we found, among the upregulated genes, desaturases SCD1 and FADS1, two enzymes that catalyze rate-limiting steps of fatty acid unsaturation through the introduction of double bonds at the delta-9 and -5 positions, respectively. Enrichment in SCD1 and FADS1 desaturases was confirmed by RT-qPCR performed on isolated CA9+/HRE− cells isolated from 3D FaDu spheroids (Fig. 2f). In 6.5/FaDu cancer cells, we similarly found a significant increase in transcript abundance of SCD1 and FADS1 (Fig. 2g); the expression of FADS2 and SCD5 was also increased in 6.5/FaDu cancer cells (Fig. 2g). A similar increase in desaturase expression was found in 6.5/HCT116 and 6.5/Siha cancer cells (Fig. S2c).

SCD1 genetic silencing and pharmacological inhibition reduce the survival of CA9-positive cancer cells

Since SCD1 was the most consistently upregulated desaturase in different acid-exposed cancer cells, we next tracked the effects of a

https://doi.org/10.1038/s41467-024-54435-3

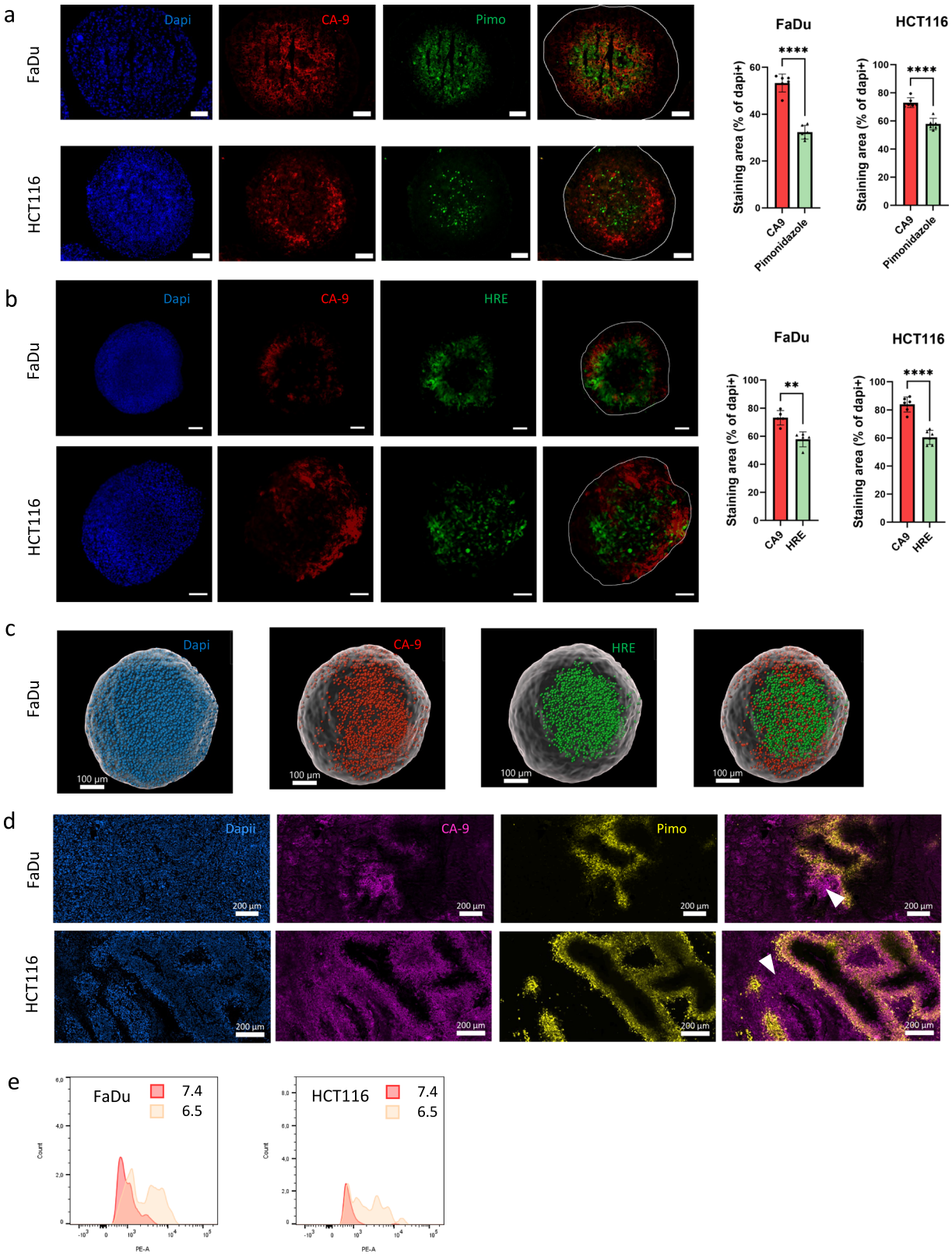

reduction in SCD1 activity in 3D spheroid models wherein acidic and non-acidic cancer cells co-exist. We first examined the effect of SCD1 silencing using the CRISPR-Cas9 system. Three distinct clones, derived from different sgRNA combinations, were selected based on their ability to induce varying levels of gene knockout (KO). (Fig. S3a). We found that SCD1 silencing led to significant growth inhibitory effects as determined based on a reduction in FaDu spheroid size and/or appearance of a halo of dead cells (Fig. 3a, b). Strikingly, when looking at an early time (i.e., before significant differences in spheroid size), CA9 expression was reduced in proportion to the reduction in SCD1 expression (Figs. 3c–e and S3b). Similar results were obtained using spheroids generated from FaDu cancer cells transduced with a plasmid encoding for SCD1 shRNA (Fig. S3c–e).

Fig. 1 | CA9 expression does not overlap with hypoxia. a Representative pictures and quantification of Carbonic Anhydrase 9 (CA9, red) and pimonidazole (green) immunostaining in FaDu and HCT116 spheroid sections ($N = 3$, $n = 2$); DAPI (blue) nuclear staining was used to normalize measurements. The white delimitation represents the rim of the spheroid. **b** Representative pictures and quantification of CA9 (red) and Hypoxia-Responsive Element-dependent GFP reporter (HRE, green) wholemount fluorescence in FaDu and HCT116 spheroids ($N = 5$ and 7, respectively). **c** 3-dimensional modeling of CA9 (red), HRE-GFP (green), and DAPI (blue) staining in Fadu spheroids; this experiment was repeated twice with similar results. **d** Representative CA9 (purple) and pimonidazole (yellow) immunostaining in FaDu and HCT116 tumor sections; this experiment was repeated twice with similar results. **e** Representative flow cytometry analysis of CA9 staining in FaDu and HCT116 cancer cells maintained under normoxia at physiological pH 7.4 or at acidic pH 6.5; this experiment was repeated twice with similar results. The scale bar represents 100 μm for 3D tumor spheroids (**a**–**c**) and 200 μm for mouse tumor sections (**d**). Data are plotted as the means ± SD (**$P = 0.0017$, ****$P < 0.0001$); N indicates the number of independent experiments and n indicates the number of biological replicates (when >1). Significance was determined by two-sided Student's t-test (**a**, **b**). Source data are provided as a Source Data file.

We also observed a net growth inhibitory effect on established spheroids upon exposure to SCD1 inhibitor (SCD1i) A939572, as determined based on reduction in FaDu spheroid size (Fig. 3f) and increased cytotoxicity as determined using IncuCyte detection of Cytotox Green Reagent accumulation (Fig. 3g). Similar results were obtained with colorectal HCT116 and HT-29 spheroids (Fig. S3f, g). Also, propidium iodide labeling confirmed that cell death was more prominent inside the spheroid wherein CA9 was expressed before exposure to SDCi (Fig. S3h). As observed with SCD1-silenced cancer cells, we found that as soon as 72 h after SCD1i exposure (i.e., before significant alterations in spheroid size), a dramatic reduction in the pool of CA9-positive cells could be detected by immunofluorescence (Figs. 3h, i and S3i) or flow cytometry from treated 3D spheroids (Fig. 3j). Interestingly, this reduction in SCD1 expression was associated with a decrease in the abundance of lipid droplets (LD) as evidenced using PLIN2 staining (Fig. S3j).

While SCD1i-induced cell death could account for the loss of CA9 signal from killed acidic cancer cells, we also examined whether the reoxygenation process occurring after SCD1i exposure could also contribute to the reduction of CA9 expression. Pimonidazole staining confirmed the reduction in the hypoxic core of FaDu and HCT116 spheroids (see green staining in Figs. 3h and S3i, quantification in Figs. 3k and S3i) in response to SCD1i treatment. Seahorse experiments further validated that SCD1i exposure reduces OCR in 3D spheroids (Fig. 3l) and in acid-adapted cancer cells (Fig. S3k). We found a similar reduction in OCR using SCD1-silenced cancer cells (Figs. 3m and S3l), also supported by a reduction in pimonidazole staining in spheroids generated from these cells (Fig. S3d, e). Conversely, supplementation of spheroids with stearate as a source of SFA led to an increased extent of CA9 and pimonidazole staining (Fig. S3m). We also showed that the O_2-dependent enzymatic activity of SCD1 could contribute to OCR and thus lead to spheroid reoxygenation upon SCD1 inhibition. For this purpose, we used SCD1-overexpressing cancer cells (Fig. S3n) and showed that non-mitochondrial OCR was significantly increased in response to palmitate as an exogenous source of SFA (Fig. 3n). Altogether these data indicate that the disappearance of CA9 signal in spheroids upon SCD1 blockade or silencing results from the preferential killing of cancer cells residing in the acidic compartment, along with a global reoxygenation process.

The preferred uptake of fatty acids that we previously reported to occur in acid-adapted cancer cells[11,15,23] led us to examine the role of the PPAR transcription factor. Interestingly, PPAR-γ inhibitor (but not PPAR-α inhibitor) led to SCD1 downregulation and recapitulated the phenotype observed upon alteration in SCD1 expression or activity, namely the extinction of CA9 and pimonidazole staining (Figs. 3o–r and S3o).

The obligatory SCD1 expression for the survival of acid cancer cells is void upon DHA exposure

While the above data identified the requirement to desaturate FA as a vulnerability associated with the enhanced FA metabolism in acid-exposed cancer cells, we then reasoned that supplementation with PUFA could further increase the stress level in these cells. This strategy is further supported by the observed SCD1i-induced reduction in LD (Fig. S3j) while PUFA excess is known to stimulate LD formation[23]. We found that n-3 PUFA docosahexaenoic acid (DHA) further enhanced the preferential cytotoxic effects of SCD1 inhibitor (SCD1i) A939572 in 3 out of 4 6.5/cancer cells (vs. corresponding 7.4/cancer cells) (Figs. 4a and S4a). In 6.5/Fadu cancer cells, DHA-enhancing effects were revealed upon the combination of SCD1i with an inhibitor of FADS1 (FADS1i) (but not FADS2i) (Figs. 4a and S4a). In parallel, we found that DHA additionally heightened the elevated levels of triacylglycerol (TAG) induced by acidic conditions (Fig. 4b). However, while the abundance of the most prominent MUFA (i.e., C18:1 oleate) was directly proportional to the TAG increase in acid-exposed cancer cells (compare black and white bars in Fig. 4b, c), DHA exposure did not further increase the oleate contribution in TAG (compare black and red bars in Fig. 4c). The increase in total TAG levels in 6.5/cancer cells mostly resulted from the incorporation of C22:6 DHA (Fig. 4c). A more detailed analysis of the composition of TAG revealed that DHA emerges as the predominant constituent of TAG, with 45% of them incorporating at least one DHA, while the TAG content in C18:1 oleate decreased from 46% to 22% in acid-exposed cancer cells (Fig. S4b). In the same experimental conditions, Bodipy staining revealed that the presence of lipid droplets was increased in 6.5/cancer cells and further enhanced in the presence of DHA (Fig. S4c, d). More importantly, while acidic pH and DHA exposure independently increased the amounts of TAG to a similar extent (see black and orange bars in Fig. 4b), the PUFA/MUFA ratio in the neutral lipid (NL) fraction was increased by 5-fold in the DHA condition (see black and orange bars in Fig. 4d). The PUFA/MUFA ratio eventually peaked in the NL but also phospholipid (PL) fractions of acid-exposed cancer cells when subjected to DHA treatment (see red bars in Fig. 4d, e).

Collectively, the aforementioned data suggested that despite SCD1 upregulation in response to an acidic environment, there is not enough MUFA to counterbalance the increased uptake of PUFA and the associated risk of membrane lipid peroxidation[23]. We next examined the reason for this paradox and found that remarkably, although SCD1 was consistently increased in acidic 6.5/cancer cells vs. 7.4/cancer cells (Fig. 4f), DHA reduced the expression of SCD1 in control 7.4/cells and also limited its upregulation in response to acidosis (Fig. 4f, g). Upregulation of SCD1 under acidosis as well as the blunting effect of DHA on desaturase expression were both confirmed by Western blotting (Fig. 4h). Collectively, these data confirm that cancer cells are particularly susceptible to SCD1 inhibition under conditions of both acidosis and DHA exposure, as acidosis stimulates desaturase expression while DHA suppresses it.

SCD silencing or inhibition exerts tumor growth inhibitory effects in mice, an effect further exacerbated by lipid metabolism rewiring in response to a PUFA-rich diet

To validate in vivo the above findings, we first compared tumor growth using SCD1-silenced clones and confirmed a significant tumor growth delay (Fig. 5a) and prolonged mouse survival (Fig. 5b). Since genetic silencing of SCD1 reduced the growth of tumors from early time, we next evaluated pharmacological inhibition of SCD1 in established tumors in mice fed a control diet or an isocaloric omega-3 PUFA-rich

https://doi.org/10.1038/s41467-024-54435-3

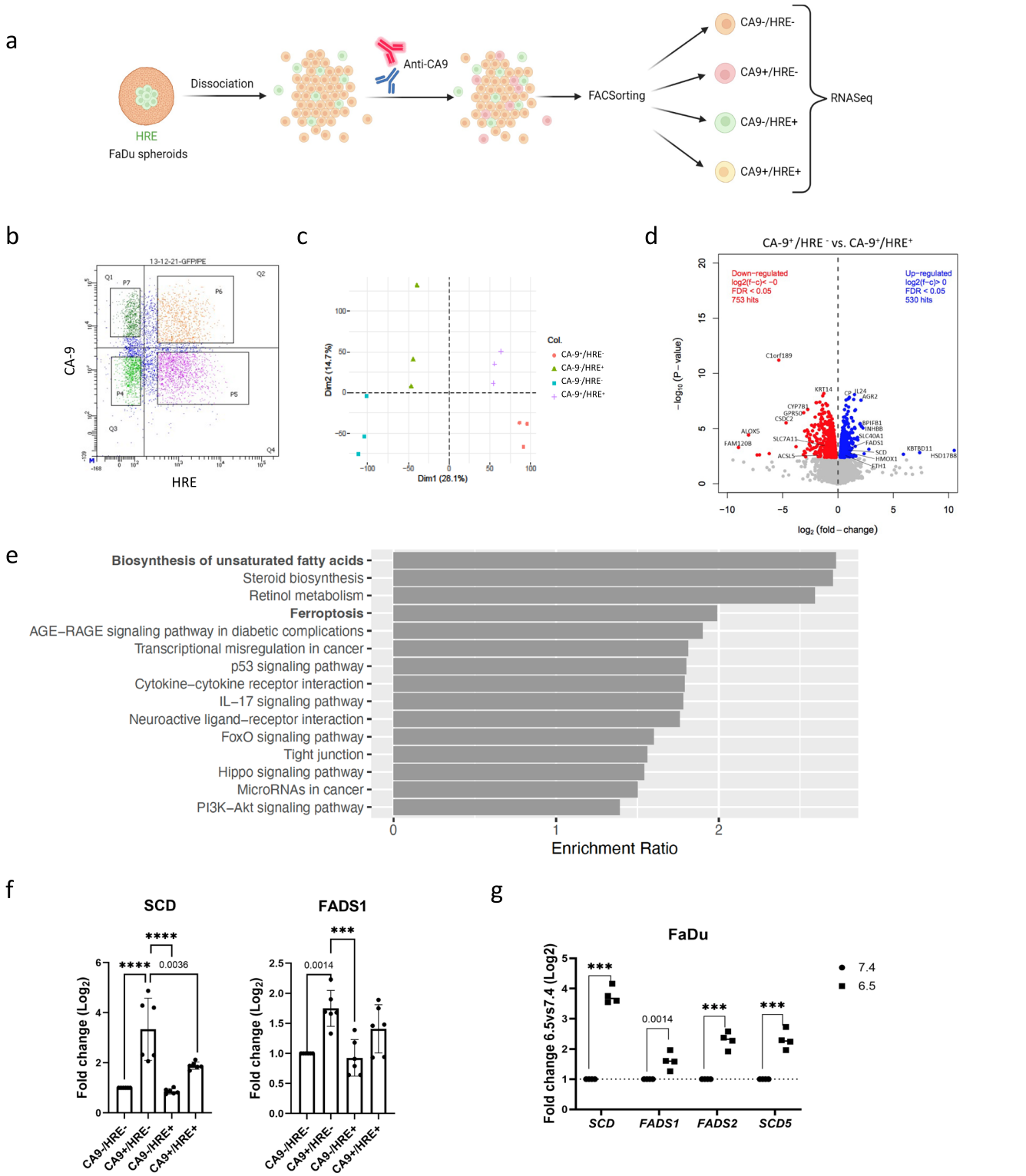

Fig. 2 | CA9-positive HRE-GFP-negative cancer cells exhibit enrichment in FA desaturase activity. a, **b** Schematic protocol of cell sorting from 3D FaDu spheroids based on CA9 immunostaining and HRE-GFP expression, created in BioRender. Feron, O. (2024) BioRender.com/i40c288 (**a**) and representative FACS plots showing gating strategy for each of the four quadrants (**b**). **c** Principal component analysis (PCA) discriminating the four quadrants based on RNA-seq analysis performed on 3 independent sorting experiments. **d** Volcano plot of differentially expressed genes between CA9+/HRE− and CA9+/HRE+ FaDu cell populations. **e**. KEGG pathway enrichment analysis of the differentially expressed genes between CA9+/HRE− and CA9+/HRE+ FaDu cell populations. **f**, **g** Changes in the mRNA expression of the indicated desaturases in the four distinct FaDu spheroid compartments (**f**) ($N = 3$, $n = 2$), and in FaDu cancer cells maintained at physiological pH 7.4 or at acidic pH 6.5 (**g**) ($N = 4$); results are expressed as fold-change *vs.* mRNA levels in CA9-/HRE- double negative cell populations and in cancer cells at pH 7.4, respectively. Data are plotted as the means ± SD (*P*-values as indicated or $^{***}P < 0.001$, $^{****}P < 0.0001$); *N* indicates the number of independent experiments and *n* indicates the number of biological replicates (when >1). Significance was determined by a two-sided Student's *t*-test with FDR adjustment (**d**), one-way ANOVA with Tukey's multiple comparison test (**f**), or two-sided Student's *t*-test (**g**). Source data are provided as a Source Data file.

https://doi.org/10.1038/s41467-024-54435-3

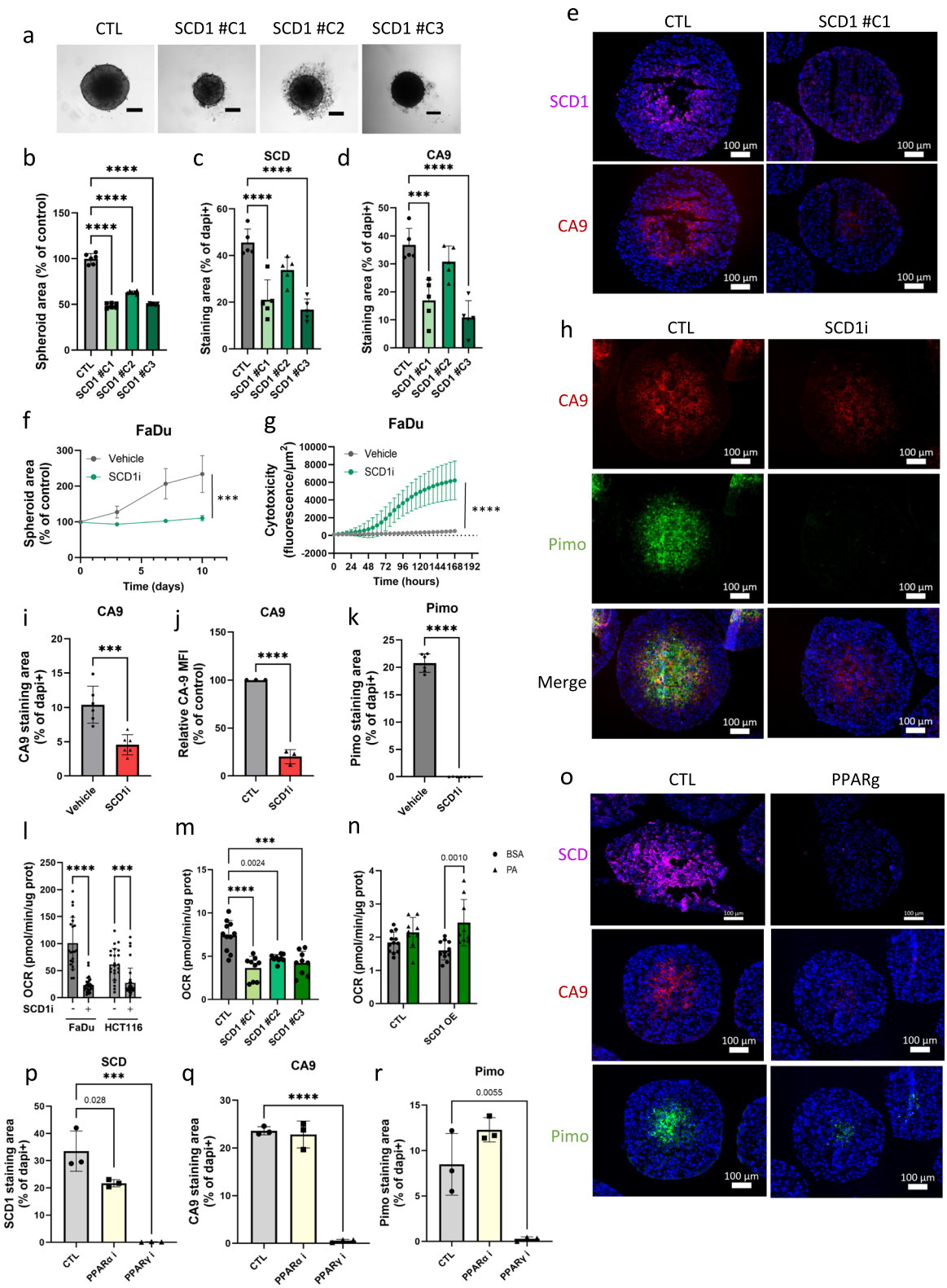

diet. The combination of the PUFA-rich diet and SCD1 inhibition significantly enhanced the extent of tumor growth inhibition (Fig. 5c) and prolonged mouse survival (Fig. 5d) whereas SCD1i treatment in mice fed the control diet did not reveal significant differences (Fig. 5c, d). Of note, in the absence of SCD1i treatment, tumor growth was slightly slowed down in mice fed PUFA-rich diet (*vs.* control diet) (Fig. 5c, d).

To get more insights into the influence of the PUFA-rich diet on the extent of SCD1 inhibition, we next examined the profiles of neutral lipids (NL) in mouse tumors (*vs.* mice fed the control diet). In the absence of treatment, the amounts of FA in the neutral lipid (NL) fraction were increased in mice on the PUFA-rich diet, regardless of their nature (i.e., SFA, MUFA and PUFA) (Fig. 5e). Strikingly, while SCD1 inhibition led to a reduction in NL content in mice fed the PUFA-rich diet, a significant accumulation of NL was observed in mice fed the control diet (Fig. 5e). Moreover, while the PUFA-rich diet globally increased the amount of PUFA in NL regardless of SCD1i treatment

Fig. 3 | SCD1 genetic silencing and pharmacological inhibition reduce the survival of CA9-positive cancer cells. a, **b** Representative contrast phase pictures (**a**) and quantification (**b**) of the effects of CRISPR-Cas9-based SCD1 gene invalidation on FaDu spheroid growth at day 7 post-formation (vs. control sgRNA); $N = 3$, $n = 2$. **c**–**e** Quantification of SCD1 (violet) (**c**) ($N = 5$) and CA9 (red) immunostaining (**d**) ($N = 5$), and representative pictures (**e**) of spheroids made of CRISPR-Cas9-based SCD1-silenced FaDu cells at day 10 post-formation. **f**, **g** Spheroid growth (**f**) ($N = 3$, $n = 3$–4) and cytotoxicity (Incucyte Cytotox Green reagent) follow up (**g**) ($N = 3$, $n = 4$) after exposure to SCD1 inhibitor (or vehicle) for 72 h in FaDu spheroids. **h**, **i** Representative pictures (**h**) and quantification of CA9 (red) (**i**) in sections of FaDu spheroids collected after 72 h exposure to SCD1 inhibitor ($N = 3$, $n = 2$). **j** Flow cytometry analysis of CA9 labeling from FaDu cells isolated from spheroids after 72 h exposure to SCD1 inhibitor (or vehicle) ($N = 3$). **k** Quantification of pimonidazole (green) in sections of FaDu spheroids collected after 72 h exposure to SCD1 inhibitor ($N = 3$, $n = 2$). **l**, **m** Mitochondrial oxygen consumption rate (OCR) of **l** FaDu ($N = 3$, $n = 7$) and HCT116 ($N = 3$, $n = 7$–8) spheroids after 72 h SCD1 inhibition and (**m**) FaDu cancer cells transduced with the indicated SCD1 sgRNA ($N = 3$, $n = 3$) or control sgRNA ($N = 3$, $n = 3$–4). **n** Non-mitochondrial OCR of FaDu cells transduced with an SCD1-expressing vector or control plasmid and exposed to palmitate ($N = 3$, $n = 3$) or vehicle (FA-free BSA) ($N = 3$, $n = 4$). **o**–**r** Representative pictures (**o**) and quantification of SCD1 (violet) (**p**), CA9 (red) (**q**), and pimonidazole (green) (**r**) staining in FaDu spheroids exposed to PPAR-γ inhibitor (or vehicle) for 72 h ($N = 3$); the effects of a PPAR-α inhibitor are also shown in graphs (**p**–**r**). All treatments (**f**–**l**) with SCD1 inhibitor (A939572, 32 μM) were initiated at day 7 after spheroid formation (i.e., timing 0 on graphs). All immunostaining quantifications (**c**, **d**, **i**, **k**, **p**–**r**) were normalized to the DAPI nuclear staining area. Data are plotted as the means ± SD (*P*-values as indicated or ***$P < 0.001$, ****$P < 0.0001$); *N* indicates the number of independent experiments and *n* indicates the number of biological replicates (when >1). Significance was determined by one-way ANOVA with Tukey's multiple comparison tests (**b**–**d**), Dunnet's multiple comparison tests (**p**–**r**), Sidaks's multiple comparison tests (**f**, **g**), two-way ANOVA with Tukey's multiple comparison tests (**l**–**n**) or two-sided Student's *t*-tests (**i**–**k**). Source data are provided as a Source Data file.

(Fig. 5f), changes in PUFA concentrations marginally influenced the total amounts of NL (see Fig. 5e). The opposed effects of SCD1 inhibition on the NL profile could actually be attributed to alterations in MUFA (Fig. 5g, compare bars 1 *vs.* 2, and 3 *vs.* 4). SCD1 inhibition led to a 3-fold reduction in the amount of MUFA in the NL fraction of tumors from mice fed the PUFA-rich diet whereas a 30% increase in MUFA was observed in the same NL fraction of tumors fed the control diet (Fig. 5g). A significant increase in SFA in the NL fraction was also observed in tumors of SCD1i-treated mice fed the control diet (Fig. S5a). The differential contribution of FA to NL accounted for a net increase in the n-3 PUFA/MUFA ratio in mice fed the PUFA-rich diet, an effect further exacerbated in the presence of SCDi (Fig. 5h). This n-3 PUFA/MUFA ratio was not significantly altered in tumors of SCDi-treated mice under control diet conditions (Fig. 5h). Remarkably, this difference was also very pronounced in the phospholipid (PL) and free FA (FFA) fractions (Fig. 5i-j). In these fractions, the n-3 PUFA/MUFA ratios were more largely increased in the presence of SCD1i reaching values up to 2-fold higher than in tumors of untreated PUFA-fed mice (Fig. 5i, j). Overall, these data suggest that the increased uptake of fatty acids (including MUFA) enables cancer cells to survive when MUFA synthesis is inhibited and that this rescue process is overwhelmed in the presence of PUFA (along with further reinforcement of SCD1 downregulation).

SCD inhibition is partly compensated by exogenous MUFA but exerts bystander cytotoxic effects on hypoxic cancer cells

The absence of MUFA reduction in the NL fraction of tumors of mice fed the control diet and treated with SCD1i led us to examine the possible compensatory contribution of exogenous MUFA and whether it could partly mitigate the therapeutic effects of SCD1 inhibition in mice fed the DHA-rich diet. To explore this hypothesis, we first used patient-derived tumor organoids (PDTO) to evaluate (in a more tractable model than mouse tumors) the capacity of oleate supplementation to reduce DHA-induced cytotoxicity. We found that DHA-exacerbated cytotoxic effects of SCD1 inhibition were indeed reversed by oleate (Fig. 6a, b). Similarly, using pH-adapted cancer cells, we found that oleate abrogated cytotoxic effects of the combo SCD1i and DHA at pH 7.4 (Fig. S6a) and partially reversed them at pH 6.5 (Fig. 6c). We further proved that the combination of SCD1i and DHA led to enhanced ferroptosis in acid-adapted FaDu and HCT116 cancer cells as revealed using Bodipy-C11 as a reporter of peroxidation (Figs. 6d and Fig. S6b for quantification). Interestingly, in the same set-up, the addition of exogenous oleate partially prevented ferroptosis, comparable to the effects of the ferroptosis inhibitor α-tocopherol (Figs. 6d and S6b).

In 3D spheroids, in the absence of an exogenous source of PUFA, we also found that the reduction in the pool of CA9+ cancer cells observed in response to SCD1 inhibition was attenuated upon oleate supplementation (Fig. 6e). Although obtained by adding excess oleate, these data indicate that exogenous MUFA has the potential to, at least in part, compensate for the deficit in MUFA synthesis and thereby possibly support partial resistance of cancer cells to SCD1 inhibition. Still, the net tumor growth inhibition observed in mice led us to search for a potential bystander effect, i.e. a phenomenon where cells that are not directly targeted by SCD1 inhibition could be nonetheless affected as a result of interactions with nearby treated acid-exposed cells.

We reasoned that an increased uptake of MUFA in response to desaturase inhibition should lead to a steeper gradient in MUFA availability in tumors. The consequence could be lipid starvation for cancer cells the most distant from the tumor blood vessels. To explore this hypothesis, we first tracked the uptake of TopFluor-OA into acid-exposed cancer cells in the presence of oxygen or under hypoxia. We found that the efficiency of OA uptake tends to be lower in hypoxic cancer cells than in non-hypoxic acid-exposed cancer cells and, importantly, that SCD inhibition led to the accumulation of significantly larger OA amounts in the latter than in hypoxic cancer cells (Figs. 6f and S6c). Hypoxic cells could thus suffer in vivo from a reduction in MUFA availability resulting from an increased uptake by acidic (non-hypoxic) cancer cells (see the model in Fig. 6g). Since the verification of this hypothesis could be biased by the reduction in tumor size, we designed an in vitro experiment wherein acidic cancer cells were exposed to SCD1i in the presence of a 1:1 mixture of OA and PA and supernatants were collected after 24 h. We found that the resulting conditioned medium (CM) led to significant growth inhibitory effects in hypoxic cancer cells (*vs.* CM from untreated acidic cancer cells) (Fig. 6h) while CM supplementation with OA rescued the survival of hypoxic cancer cells (Fig. 6h). Strikingly, direct exposure of hypoxic cancer cells to SCD1i did not induce cytotoxicity (Fig. 6h), in agreement with the need of O_2 to support SCD1 enzymatic activity[26]. Measurements of FA concentrations confirmed that CM of acidic cancer cells exposed to SCD1i were deprived in MUFA (Fig. 6i) and exhibited a net increase in the SFA/MUFA ratio (Fig. 6j) more prone to induce apoptosis in hypoxic cancer cells. This is further supported by an SCD1i-triggered increase in ATF3 staining (previously identified as a very sensitive ER stress marker resulting from SFA toxicity[27]) which accompanies the reduction in CA9 staining (Fig. S6d).

Discussion

CA9 may exert a dual role by facilitating CO_2 hydration into bicarbonate and H^+, or alternatively, by managing excess (glycolytic) H^+ through CO_2 venting[18,28]. On the premise that all tumor cells located at the same distance from the center of a spheroid share the same phenotype, we were able to isolate a population of cells harboring CA9

https://doi.org/10.1038/s41467-024-54435-3

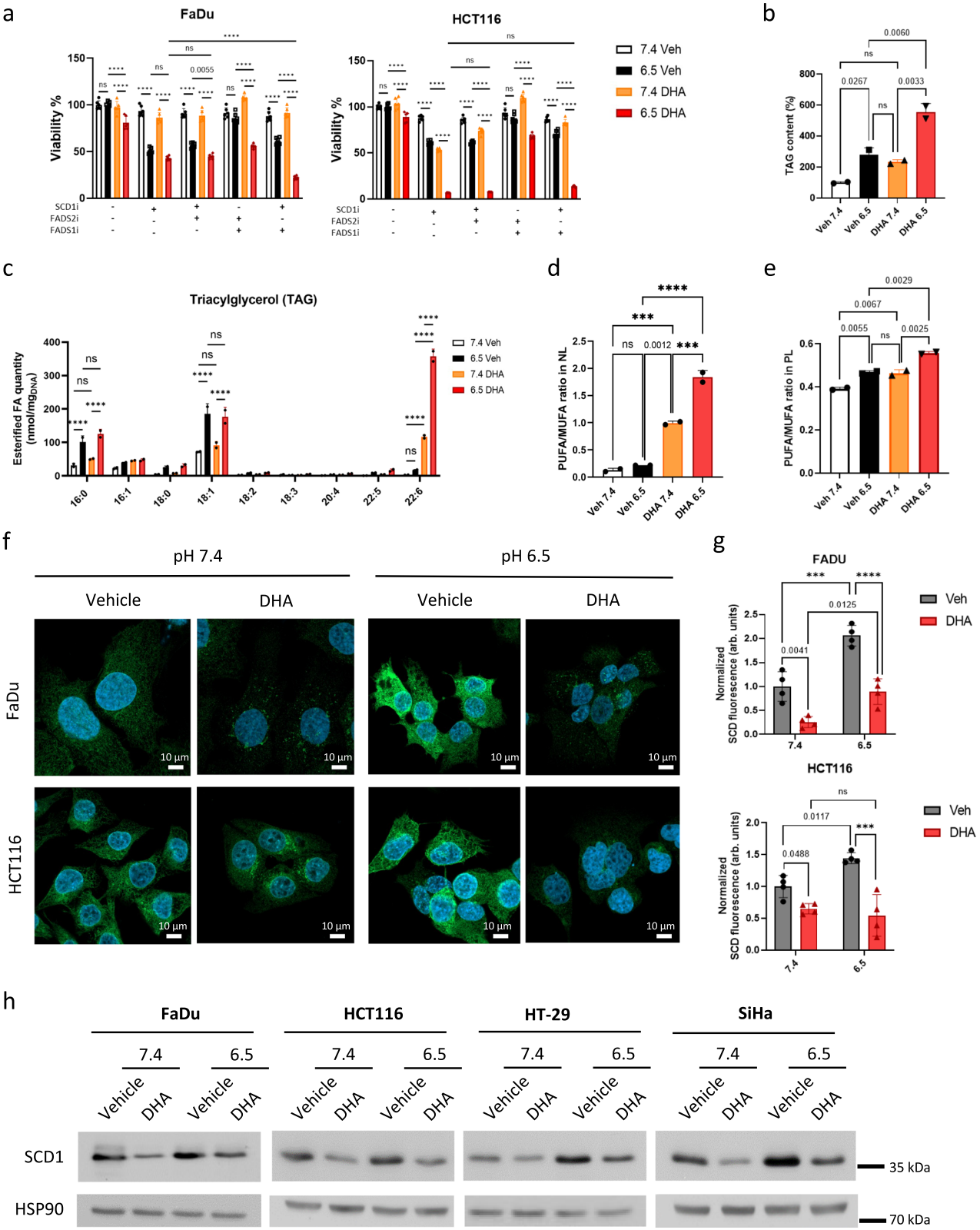

expression but not facing deep hypoxia as detected by using pimonidazole or HRE-GFP reporter. The enrichment of the MUFA biosynthesis pathway in these cells enabled us to reveal a major role for FA desaturases in the survival of non-hypoxic, acid-exposed cancer cells. Pharmacological inhibition and genetic silencing of SCD1 desaturase, the rate-limiting enzyme in MUFA synthesis, both identified the loss of the CA9+ cell population in 3D spheroids as an early event in the observed growth inhibitory effects. This observation prompted us to unveil two major phenomena with major therapeutic consequences: (i) the absolute requirement of MUFA to detoxify PUFA accumulation when cells concomitantly face an acidic environment, and (ii) a symbiotic relationship between acid and hypoxic tumor compartments, the latter being dependent on the uptake of exogenous MUFA not consumed by the former. The combination of these two findings

Fig. 4 | The obligatory SCD1 expression for the survival of acid cancer cells is void upon PUFA exposure. a Effects of inhibitors of SCD1 (A939572), FADS2 (SC-26196), and FADS1 (T3364366) on the viability of 7.4/ and 6.5/cancer cells (48 h, 32 μM for single-inhibitor treatment or 16 μM of each inhibitor for combination) in the presence of 50 μM DHA or vehicle (FA-free BSA) ($N = 3$, $n = 2$). **b**–**e** Lipidomic analysis of 6.5/ and 7.4/HCT116 cancer cells after 24 h exposure to 25 μM DHA or vehicle ($N = 2$). **b** Triacylglycerol (TAG) content expressed as % of the value measured in 7.4/cells, **c** TAG composition in esterified FA, **d**, **e** PUFA/MUFA ratio in neutral lipid (**d**) and phospholipid (**e**) fractions. **f**, **g** Representative pictures (**f**) and quantification (**g**) of SCD1 (green) immunofluorescence signal in the indicated 7.4/ and 6.5/cancer cells exposed or not to 20 μM DHA for 72 h ($N = 4$). **h** SCD1 immunoblotting from the indicated 6.5/ and 7.4/cancer cells exposed or not to 20 μM DHA for 72 h ($N = 1$). Data are plotted as the means ± SD (ns: non-significant, P-values as indicated or ***$P < 0.001$, ****$P < 0.0001$); N indicates the number of independent experiments and n indicates the number of biological experiments (when >1). Significance was determined by one-way ANOVA with Tukey's multiple comparison test (**b**–**e**, **g**) or two-way ANOVA with Tukey's multiple comparison test (**a**). Source data are provided as a Source Data file.

substantiates the anticancer synthetic lethality of combining PUFA-rich diet and SCD1 inhibition.

Our lipidomic study first revealed that the capacity of MUFA to support TAG formation to incorporate PUFA (and thereby reduce the risk of peroxidation)[23] was altered under acidic conditions. Indeed, while acidic conditions and PUFA (i.e., DHA exposure) both increased the amounts of intracellular TAG, only acidic pHe was associated with an increase in MUFA (i.e. C18:1 oleate) in the NL fraction, mitigating the increase in PUFA/MUFA ratio otherwise observed upon DHA exposure (Fig. 4b–d). Moreover, when PUFA exposure was combined with acidic conditions, while the TAG level was significantly increased (to a larger extent than each treatment separately), the MUFA contribution did not increase further than in response to acidic pHe alone (Fig. 4b, c). As a consequence, the PUFA/MUFA ratio was yet more largely enhanced (than upon exposure to DHA alone) in the NL but also the PL fractions (Fig. 4d, e), supporting an increased sensitivity to ferroptosis (Fig. 6d). Importantly, we documented that this observation was largely dependent on the blunting of the acidosis-driven SCD1 upregulation in the presence of exogenous PUFA (Fig. 4f–h). This finding underscores the bidirectional nature of the relationship between PUFA and SCD1 since earlier studies indicated that a lack of PUFA leads to an upregulation of SCD1 expression and activity, subsequently elevating plasma triglyceride concentrations[29]. Strikingly, while a repressing PUFA-responsive element was previously identified in the SCD1 promoter region[30] and is likely to account for the SCD1 downregulation in acid-exposed cells, we found that PUFA-sensitive PPAR transcription factor largely drives SCD1 regulation in these cells, as previously reported in the liver[31]. It is likely that a biphasic PUFA dose effect could explain this seemingly paradoxical regulation. Interestingly, Kondo et al. identified SREBP2 as another transcription factor highly sensitive to acute exposure to acidic pHe[32], suggesting that FA but also cholesterol metabolism are major hallmarks of tumor acidosis.

The second major finding of this study that supports synthetic lethality of the PUFA and SCD1 inhibitor combination, was related to the MUFA deprivation of hypoxic cancer cells resulting from the triggered dependency of acid-exposed cancer cells on exogenous MUFA. SCD1 activity was previously shown to be critical under specific nutrient (lipid)-compromised environments including low serum culture conditions,[33] poorly vascularized CNS niches (ie, cerebrospinal fluid)[34], and calorie restriction diet[35]. Young et al. also documented that SCD1 inhibition in normoxic cancer cells phenocopied a deficit in MUFA under hypoxia in cells exhibiting oncogenic mTOR activation[36]. MUFA supplementation (or mobilization from lipid droplets)[37] but also SCD1 upregulation have been associated with a reduction in SFA-driven ER stress[38–40], displacement (or replacement) of PUFA to reduce the risk of lipid ROS accumulation within membrane phospholipids[41] or both[24]. Our work adds the spatial dimension to the above studies by documenting that within the same tumor, attempts to compensate SCD1 inhibition by enhanced uptake of exogenous MUFA may work for one cell compartment but at the detriment of another one. We showed indeed that PUFA supplementation by dampening SCD1 expression greatly reinforces the addiction of acid-exposed cancer cells to the external MUFA source. As a consequence, upon exposure to SCD1 inhibitor, acid-exposed cancer cells avidly consume MUFA, depriving the extracellular milieu from them. This effect combined with the incapacity of SCD1 to desaturate SFA in the absence of O_2 accounts for the killing of hypoxic cancer cells unable to mitigate ER stress. This collateral impact on surrounding hypoxic cells (bystander effect) bolstered by the paradoxical response of tumor-bearing mice (fed either a control or a PUFA-rich diet) to SCD1 inhibition (i.e., increase and decrease in the tumor TAG levels, respectively) was confirmed in an in vitro model decomposing the hypoxic and acidic (non-hypoxic) cell compartments. Remarkably, our study also emphasizes the concomitance and the mutual reinforcement of two distinct modes of cell death caused by a deficit in MUFA availability in the same tumor, namely apoptosis resulting from SFA-induced ER stress[27,36,40] and alterations in cardiolipin[33] but also PUFA-driven ferroptosis in acid-exposed cancer cells (this study). In this context, it is worth noting that acid-exposed cancer cells (contrary to hypoxic cancer cells) exhibit very low basal ER stress, as indicated by ATF4 and Bip markers (Fig. S6e), supporting the beneficial effects of enhanced MUFA synthesis in these cells. This finding also aligns with the growing interest in pro-ferroptotic approaches (rather than pro-apoptotic chemotherapies) to prevent the emergence of resistance from unaltered tumor compartments[42]. More generally our work identifies SCD1 activity as a control point for the O_2 balance between different tumor regions, directly contributing to the O_2 gradient formation. Indeed, we previously reported that FAO is upregulated (concomitantly to FAS) in acid-exposed cancer cells in part through enhanced PPAR activity[11,15,23], itself responding to increased availability of FA, including MUFA. This may explain why O_2 consumption is reduced when MUFA synthesis is inhibited together with the ETC modulation upon alterations in the inner mitochondrial membrane[33] and the suppression of O_2 consumption by SCD1 itself.

Regarding in vivo therapeutic options derived from this extended knowledge of metabolic addiction of acid-exposed cancer cells, we combined the administration of SCD1 inhibitors with a dietary PUFA enrichment in line with DHA supplementation of a normal diet[23]. This combined approach repositions SCD1 inhibition as a realistic anticancer target despite the physiological compensatory response resulting from exogenous MUFA uptake. This strategy may be related to the capacity of DGAT inhibitors to prevent the formation of TAG and thereby tip the balance toward an increase in plasma membrane PUFA that increases the risk of peroxidation[23]. Interestingly, a close vicinity of SCD1 and DGAT2 was recently reported, the former promoting the channeling of MUFA to the latter[43] and indirectly supporting a preference for MUFAs in TAG synthesis.

In summary, our study identified the acidic tumor compartment as exquisitely dependent on the availability of MUFA preferentially synthesized intracellularly using desaturases such as SCD1 but also captured from the extracellular medium in response to desaturase inhibition. Our work unraveled the interruption of a symbiotic dialog between cells able to use SCD1 to generate endogenous MUFA and those lacking O_2 and thus more dependent on exogenous MUFA. Upon SCD1i exposure, the forced uptake of exogenous MUFA by the former induced cytotoxicity in the latter. On top of this, in the presence of PUFA supplementation, acidic cancer cells will also directly suffer from SCD1i, the effect of which is further reinforced by the downregulation of the enzyme expression and the consecutive increase in the PUFA/MUFA ratio prone to support ferroptosis.

https://doi.org/10.1038/s41467-024-54435-3

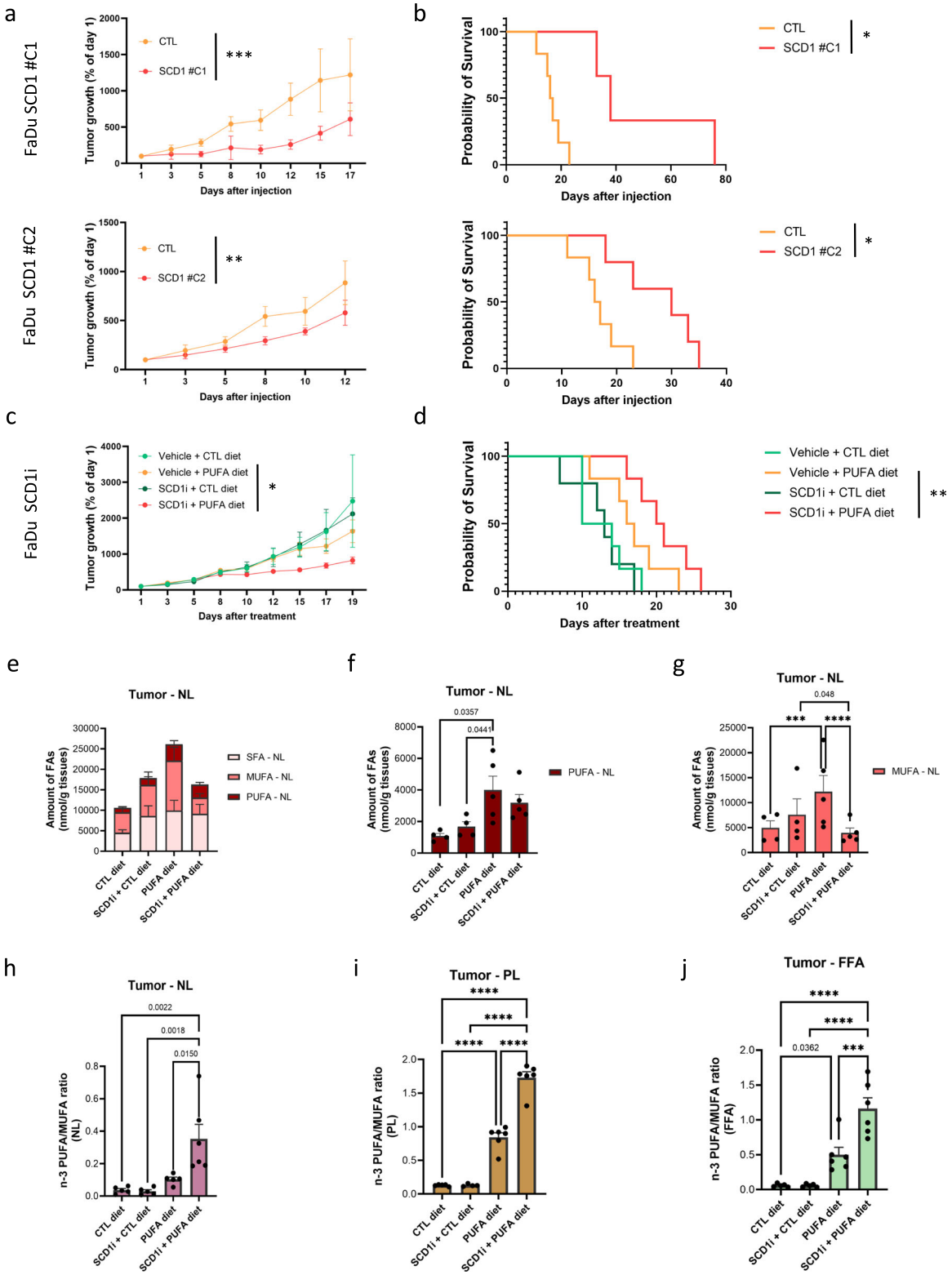

Fig. 5 | SCD silencing or inhibition exerts tumor growth inhibitory effects in mice, an effect further exacerbated by lipid metabolism rewiring in response to a PUFA-rich diet. a, **b** Tumor growth (**a**) and survival (**b**) of mice injected with SCD1 knock out FaDu cancer cells (top), clone #C1 ($n = 5$ mice per group, $^{*}P = 0.0110$, $^{***}P < 0.001$) and bottom, clone #C2 ($n = 6$ mice per group, $^{*}P = 0.0151$, $^{**}P = 0.0022$). **c**, **d** Effects of daily SCD1 inhibitor administration (A939572, 30 mg/kg) on tumor growth ($^{*}P = 0.0352$) (**c**) and survival ($^{**}P = 0.0033$) (**d**) of mice injected with FaDu cancer cells and fed with control ($n = 5$ mice per group) or PUFA-rich diet ($n = 6$ mice per group). **e**–**g** Total FA (**e**), PUFA (**f**), and MUFA (**g**) in the neutral lipid fraction of tumors from mice treated with SCD1 inhibitor and fed with control ($n = 4$) or PUFA-rich diet ($n = 5$). **h**–**j** *n*-3 PUFA/MUFA ratios in NL (**h**) ($n = 5$), PL (**i**) ($n = 6$), and FFA (**j**) ($n = 6$) fractions of tumors from mice treated with SCD1 inhibitor and fed with control or PUFA-rich diet. Data plotted as the means ± SEM (*P*-values as indicated or $^{***}P < 0.001$, $^{****}P < 0.0001$). Significance was determined by one-way ANOVA with Tukey's multiple comparison tests (**h**–**j**), two-way ANOVA (**a**) with Tukey's multiple comparison tests (**c**), or Fisher's Least Significative difference (**e**–**g**) and Long-rank Mantel–Cox test (**b**, **d**). Source data are provided as a Source Data file.

https://doi.org/10.1038/s41467-024-54435-3

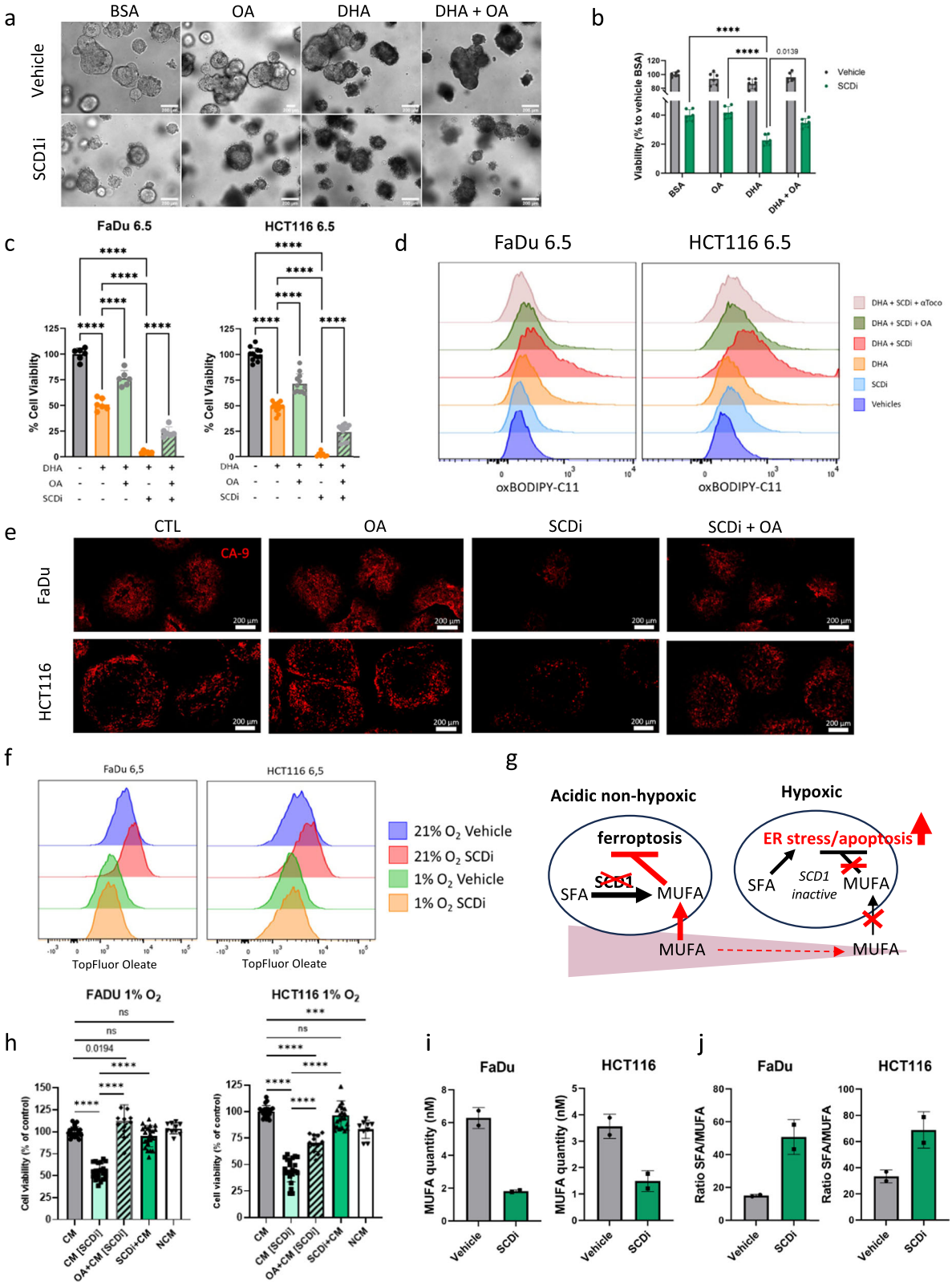

Methods

Ethical statement

This research complies with all relevant ethical regulations. Experiments involving mouse xenograft received the approval of the ethics committee from UCLouvain (approval ID 2020/UCL/MD032) and were carried out according to national care regulations.

Cell culture

Human head and neck hypopharyngeal (FaDu, HTB-43), colorectal (HCT116, CCL-247; HT-29, HTB-38), and cervix (SiHa, HTB-35) cancer cell lines were purchased from ATCC. Cell lines were stored according to the supplier's instructions and used within 6 months after resuscitation of frozen aliquots. All cells were cultured in DMEM supplemented with 10% heat-inactivated FBS, 10 mM D-glucose, 2 mM

Fig. 6 | SCD inhibition is partly compensated by exogenous MUFA but exerts bystander cytotoxic effects on hypoxic cancer cells. a, **b** Representative pictures (**a**) and quantification (**b**) of colorectal cancer patient-derived organoids after treatment with SCD1 inhibitor (A939572, 20 μM) in the presence of OA (100 μM) and/or DHA (50 μM) for 96 h ($N = 2$, $n = 2$). **c**, **d** Effect of SCD1 inhibitor (12 μM) on the viability (96 h) (**c**) and lipid peroxidation BODIPY-C11 staining (72 h) (**d**) of 6.5/Fadu ($N = 3$, $n = 2$) and 6.5/HCT116 ($N = 3$, $n = 4$) cancer cells in the presence of OA (100 μM) and/or DHA (50 μM) and/or α-Tocopherol (10 μM) or vehicle(s). **e** Representative pictures of CA9 immunofluorescence signal (red) in equatorial sections of FaDu and HCT116 spheroids exposed for 72 h to SCD1 inhibitor (A939572, 32 μM) in the presence of OA (100 μM) or not; this experiment was repeated twice with similar results. **f** Representative flow chart depicting the effects of SCD1 inhibitor on the uptake of TopFluor oleate by 6.5/Fadu and 6.5/HCT116 cancer cells maintained under normoxia or hypoxia (1% O_2) ($N = 4$, $n = 4$). **g** Schematic representation of the symbiotic relationship between hypoxic cancer cells (unable to synthesize MUFA and thus dependent on exogenous MUFA) and acidic, non-hypoxic cancer cells that may use both MUFA sources. Inhibition of SCD1 however forces the latter cell compartment to capture exogenous MUFA thereby depriving hypoxic cells from a vital source of MUFA. **h** Viability of FaDu and HCT116 cancer cells maintained under hypoxia (1% O_2) and exposed for 48 h to the conditioned medium (CM) from normoxic 6.5/FaDu and 6.5/HCT116 exposed or not to SCDi (24 h, 15 and 25 μM A939572, respectively) ($N = 3$, $n = 7$). In some experiments, CM was supplemented by oleate (50 μM) ($N = 3$, $n = 4$). Control conditions consist of CM + fresh addition of SCDi ($N = 3$, $n = 7$), and non-conditioned medium (NCM) ($N = 3$, $n = 3$). **i**, **j** MUFA amounts (**i**) and SFA/MUFA ratio (**j**) determined in the conditioned medium (CM) of normoxic 6.5/FaDu and 6.5/HCT116 cancer cells exposed or not to SCDi as above ($N = 2$). Data are plotted as the means ± SD (ns: non-significant, *P*-values as indicated or $^{***}P < 0.001$, $^{****}P < 0.0001$); *N* indicates the number of independent experiments and *n* indicates the number of biological replicates (when >1). Significance was determined by two-way ANOVA with Tukey's multiple comparison test (**b**–**h**). Source data are provided as a Source Data file.

L-glutamine (or glutamax), and if needed 25 mM of both PIPES and HEPES before adjusting pH to 7.4 or 6.5. Acidosis pH-adapted tumor cells were established as previously described[10]. All cell lines were tested for mycoplasma contamination with the MycoAlert™ Mycoplasma Detection kit (LT07-318; Lonza) before being used. After collection, cell number was assessed by cell counting on a hematocytometer with Trypan Blue mortality exclusion dye.

Cell transfection and lentiviral infection

Cell transfection of 5×HRE/GFP plasmid (#46926, Addgene) was carried out with Lipofectamine LTX with plus reagent (#15338100, Thermo Fisher Scientific), according to manufacturer's instructions. Transfected cell lines were selected with G418 treatment (2 mg/mL) for 1 week.

For CRISPRS-Cas9 gene invalidation, 15 μg of plasmids containing the constitutive Cas9 gene (VB221215-1151jyw, VectorBuilder) were transfected by Calcium Phosphate (#CAPHOS-1KT, Merck) technique in HEK293T packaging cells together with 15 μg of psPAX (#12260, Addgene) and pMD2G (#12259, Addgene) second-generation packaging plasmids by following the manufacturer's indications. The produced virions were transferred to target cell lines after filtration. After 24 h of transduction, the virion-containing media was removed and the transduced cells were selected with 8 μg/mL blasticidin for 1 week. A subsequent packaging and transduction were performed on Cas9 expressing cell lines with single guide (sg) RNA necessary for SCD1 gene invalidation at the position 43 (CCTGCTTGGCAGCGGATAAA, VectorBuilder) and 109 (GCCTTTAAATTCCCGGCTCG, VectorBuilder) of the target gene or a CTL (sg) RNA (GTGTAGTTCGACCATTCGTG, VectorBuilder), Cancer cells were infected with sg190 (C2) or a combination of sg43 and sg109 (C1 and C3). Following infection, the cells were subjected to a 1-week long puromycin selection (1 μg/mL) and a clonal selection to isolate individual clones for further analysis.

For the overexpression of SCD1 (VB900124-8400vbs, VectorBuilder) and shRNA-mediated downregulation of SCD1 (target sequence: CGTCCTTATGACAAGAACATT, VectorBuilder), second-generation packaging and transduction were performed, as previously described. Scramble controls were used for both conditions, with mRFP for overexpression and a scramble sequence (CCTAAGGTTAAGTCGCCCTCG) for downregulation. Post-transduction, cells were subjected to a 1-week selection using 1 μg/mL puromycin.

3D spheroid models

Spheroids were formed with FaDu, HCT116, and HT-29 cell lines and cultured in commercial DMEM media supplemented with 10% heat-inactivated FBS, 10 mM of D-glucose, and 2 mM of glutamax. They were seeded at a density of 1500 cells/well in 96-well ultra-low attachment plates (7007, Costar or 83.3925.400, BIOFLOAT) and cultured for 7 days before performing further experiments.

Fatty acid supplementation and treatments

Fatty acid supplementation was performed in full media with lipid-depleted FBS (S181L-500, VWR) and BSA-conjugated fatty acids at a concentration of 50 μM of docosahexaenoic acid (DHA, 10-2206, Larodan), 100 μM of palmitic acid (PA, 10-1600, Larodan) and/or oleic acid (OA, 10-1801, Larodan) during 24, 48 or 72 h. 3D spheroids were supplemented with 100 μM of DHA and OA or 50 μM of PA and SA (stearic acid, 10-1800-17, Larodan) during 24 or 72 h in full media. Fatty acids were conjugated with BSA in PBS to obtain a fatty acid/BSA ratio of 4:1 (mol:mol). Aliquoted fatty acids were stored at −80 °C under light protection and directly used upon unfreezing by the addition of the requested concentrations into the wells.

2D and 3D culture treatments were performed with full media, during 72 h with 32 μM of SCD1 inhibitor (A939572, #HY-50709, Med Chem Express) or during 24 h with 25 μM of PPARα inhibitor (GW6471, S2798, Bioconnect) and PPARγ inhibitor (GW9662, HY-16578, MedChemExpress).

Cell density was determined by using the Presto Blue reagent (Thermo Fisher Scientific) according to the manufacturer's instructions. Spheroid growth was monitored using a live-cell phase contrast microscope (Axio Observer, Zeiss) or IncuCyte automated system (#SX5, Sartorius) and the spheroid area was measured by Fiji software or IncuCyte software.

Patient-derived tumor organoids

Tumor organoids were generated from a local library of specimens collected from CRC patients undergoing surgery or tumor biopsy at Cliniques universitaires St Luc in Brussels (ethics committee approval n°ONCO-2015-02 updated on 13-05-2019 in accordance with the principles of the Declaration of Helsinki). The organoids used in this study were obtained from a male patient with CRC who did not receive any compensation. Signed informed consent was obtained before tumor collection and all personal/clinical data remained strictly confidential for the investigators. Organoids were cultured in Advanced DMEM/F12 media (Gibco) supplemented with glutamine, penicillin/streptomycin, primocin 100 μg/ml (Invivogen), B27 without vitamin A 1× (Thermo Fisher Scientific), N2 1× (Thermo Fisher Scientific), Nicotinamide 100 mM (Sigma), N-acetylcysteine 1.25 mM (Sigma) and hEGF 50 ng/ml (STEMCELL Technologies) and embedded in Cultrex BME type 2 (Biotechne), using Corning Costar 24 well plates (Ref:3524). The organoids were allowed to grow in their media at physiological pH but over the duration of the SCDi test, the organoids media was set at pH 6.9. The organoids have been treated for 96 h with vehicle or SCDi 20 μM, and the corresponding fatty acids (OA 100 μM and/or DHA

50 μM) or BSA (used in the same amounts as the fatty acids accordingly).

Immunofluorescence staining of 2D cell cultures

To perform the immunostaining of SCD1, cancer cell monolayers were washed twice with PBS and fixed with PFA 4% for 20 min at room temperature (RT). After two washes, cells were permeabilized with 0.1% saponin for 20 min at RT and washed 3 times. Then, cells were blocked with a solution of 2% BSA/ 0.05% Saponin for 1 h at RT and incubated with an SCD antibody (#ab236868, Abcam, 1:100) diluted in 0.1% BSA/ 0.05% Saponin, overnight at 4 °C. After the incubation, the cells were washed three times with cold PBS and then incubated with an Alexa Fluor 488-conjugated anti-rabbit secondary antibody (#A32790, Thermo Fisher Scientific, 1:600) and DAPI diluted in 0.1% BSA/ 0.05% Saponin, for 1 h at RT. Finally, cells were washed three times with PBS before being imaged with an LSM 800 confocal microscope (Zeiss).

To stain lipid droplets, cancer cell monolayers were washed twice with warmed PBS and incubated with 2 μM BODIPY 493/503 (D3922, Thermo Fisher Scientific) in PBS for 20 min at 37 °C and 5% CO2. After three washes, cells were fixed with PFA 4% for 20 min at RT in the dark. Cells were washed three times more with PBS and imaged with LSM 800 confocal microscope (Zeiss). 2D immunofluorescence images were analyzed with ImageJ. Briefly, each cell was delimited to create a Mask and saved as a Text Image corresponding to pixels from cells. In parallel, the same threshold was applied to all images and saved as Text Image, corresponding to interest pixels (SCD or LD staining). Using the RStudio software, interest pixels per cell were quantified.

Immunofluorescence staining of 3D spheroids

3D tumor spheroids were treated with 1 mg/mL of propidium iodide (P4170, Sigma) for 15 min or 1 μM of pimonidazole for 24 h, fixed with 4% PFA during 24 h, incubated with 30% sucrose and embedded in OCT. Frozen spheroid sections (8 μm) were permeabilized in 0,5% of PBS-Triton X-100, blocked with 5% BSA during 1 h, incubated overnight at 4 °C with anti-CA9 (#AF2188, R&D, 1:500), anti-SCD1 (#ab236868, Abcam, 1:200), anti-pimonidazole (#Pab27, HPI, 1:200), anti-ATF3 (# MA5-31360, Thermo Fisher Scientific, 1:100) or anti-PLIN2 (#HPA016607, Merck, 1:100) primary antibodies. Spheroid sections were then incubated with Alexa Fluor 488-conjugated anti-rabbit and 568-conjugated anti-goat secondary antibodies (#A32790 and #A11057, respectively; Thermo Fisher Scientific) for 1 h and nuclei were counterstained with Hoechst. Slides were prepared with fluorescence mounting medium (Dako) and the staining was visualized by AxioImager.z1-ApoTome1 (Zeiss). All spheroid samples from the same experiment were imaged with the same gain and exposure settings. Immunofluorescence results were analyzed with Zen Blue (Zeiss) and quantified with QuPath software. The tissue total area and the area of the staining of interest were measured by creating a pixel classifier with a fluorescence thresholder. The area of a staining compartment was measured by creating an annotation of the zone where the staining is present.

Wholemount immunofluorescence and Light Sheet microscopy

3D spheroids containing 5HRE/GFP plasmid were fixed with 4% PFA for 24 h, blocked, and permeabilized at 4 °C overnight in 0.5% of PBS-Triton X-100, containing 5% of BSA. Whole spheroids were incubated with the anti-CA9 primary antibody (#AF2188, R&D, 1:500) at 4 °C for 5 days under shaking and then incubated with 568-conjugated anti-goat secondary antibody (#A11057, Thermo Fisher Scientific) and Hoechst at 4 °C for 4 days, under shaking. The antibody incubation was followed by 2 h of 4% PFA fixation and spheroid clearing with CUBIC 1 for 4 days and CUBIC 2 for 3 days. CUBIC1 and 2 were prepared by following the instructions of Susaki et al.[44]. Spheroids were mounted into 1% agarose in capillaries and visualized with Lightsheet.z1 (Zeiss). All spheroid samples from the same experiment were imaged with the same gain and exposure settings. Immunofluorescence results were analyzed with Zen Blue (Zeiss), modelized with Imaris software, and quantified with QuPath software.

Multiplex immunofluorescence in tumor sections

Tumors collected from mice were fixed with 4% PFA for 48 h and embedded in paraffin. Paraffin tumor sections (5 μm) were deparaffinized with 3 consecutive baths of toluene and isopropanol. Endogenous peroxidases were inactivated with 3% H_2O_2 diluted in 40% isopropanol. Before each primary antibody staining, antigen retrievals of tumor sections were performed with citrate buffer, followed by permeabilization with 0.1% of TBS-Tween 80 and blocking with 5% BSA for 1 h. Consecutive primary antibody stainings were performed with anti-pimonidazole (#Pab27, HPI, 1:1000), anti-PLIN2 (#HPA016607, Merck, 1:100) and anti-CA9 (#AF2188, R&D, 1:500) antibodies during 1 h at RT. Slides were then incubated with anti-rabbit-HRP or anti-goat-HRP secondary antibodies (#K4003, Dako, ready to use; #705-035-147, Jackson Immuno Research, 1:100) during 40 min, followed by a 10 min incubation with Alexa Fluor 555-(B40955, Thermo Fisher Scientific, 1:200), Alexa Fluor 488- (#B40953, Thermo Fisher Scientific, 1:200) and Alexa Fluor 750-coupled (#B56131, Thermo Fisher Scientific, 1:1000) tyramide diluted in borate buffer with 0.003% H2O2, respectively. Nuclei were counterstained with Hoechst, slides were prepared with fluorescence mounting medium (Dako) and acquired with Axioscan.z1 (Zeiss). All tumor samples from the same experiment were imaged with the same gain and exposure settings. Immunofluorescence results were analyzed with Zen Blue (Zeiss) and quantified with QuPath software.

Flow cytometry and FACSorting

6.5 and 7.4 pH-adapted 2D cell lines were collected and stained with PE-coupled anti-CA9 antibody (130-123-340, Miltenyi, 1:200) for 20 min at 4 °C. To assess viability, cells were incubated with DAPI before acquisition. 3D spheroids were harvested and dissociated with Accumax (07921, STEMCELL) or Accutase (07922, STEMCELL) at RT under shaking for 10 min. The staining was performed with PE-coupled anti-CA9 antibody (130-123-340, Miltenyi, 1:200) for 20 min at 4 °C. To assess viability, cells were incubated with DAPI before acquisition. After incubation, cells were acquired by flow cytometry on FACSCanto II (BD Biosciences) or sorted with FACSAria III (BD Biosciences) with a gating strategy excluding debris, double cells, and dead cells.

For BODIPY-C11, 6.5 pH-adapted cell lines were treated with SCDi (12 μM) and/or DHA (50 μM) in the presence or not of OA (100 μM) or α-Tocopherol (20 μM) (#T3634, Sigma Aldrich). After 72 h, the cells were harvested and incubated with 2 μM of BODIPY-C11 (#D3861, Thermo Fischer Scientific) for 30 min at 37 °C. After incubation, cells were acquired by flow cytometry on FACSCanto II (BD Biosciences) with FITC channel corresponding to oxidized BODIPY-C11.

For TopFluor-OA, 6.5 pH-adapted cell lines were plated at 40% confluence and maintained in Normoxia or Hypoxia (1% O_2). After 24 h, cells were treated with SCDi (12 μM) for 24 h. Then, cells were incubated with 2 μM TopFluor-OA (810259, Avanti Research) in a serum-free medium for 30 min at 37 °C (still in normoxia or hypoxia). After incubation, cells were acquired by flow cytometry on FACSCanto II (BD Biosciences) with a FITC channel.

Flow cytometry analysis was performed with the FlowJo software.

RNA Sequencing analysis

1 million cells per condition were isolated from spheroids by FAC-Sorting. The RNA quantity and quality evaluation, the RNA extraction, and the RNA Sequencing were performed at Marcogen. Briefly, samples (biological triplicates) were prepared with the TruSeq Standarded mRNA Library Prep Kit (#20020594; Illumina) from 1 μg RNA. The sequencing was performed using the NovaSeq 6000 Sequencing

system with paired-end reads, all according to the manufacturer's recommendations. All RNA-sequencing data were analyzed by using the Automated Reproducible MOdular workflow for preprocessing and differential analysis of RNA-seq data (ARMOR v1.5.4) pipeline. In this pipeline, reads underwent quality control with FastQC (Babraham Bioinformatics). Quantification and quality control results were summarized in a MultiQC report before being mapped to the human transcriptome using Salmon, which was built by applying all Ensembl cDNA sequences obtained in the Homo_sapiens.GRCh38.cdna.all.fa file. Next, estimated transcript abundances from Salmon were imported into R using the tximeta package and analyzed for differential gene expression with edgeR. Over Representation Analysis (ORA) and Gene Set Enrichment Analysis (GSEA) were performed with the WebGestaltR v.0.4.4 Bioconductor package on the KEGG, GO, and HALLMARKS databases. Raw and processed RNA-seq data were deposited and made publicly available on the Gene Expression Omnibus.

Lipid analysis

Lipid extraction from cultured cancer cells and collected tumor samples and data analysis methods were previously described. Briefly, gas chromatography-flame ionization detection (GC-FID) was used to quantify fatty acids as phospholipids, neutral lipids, and free fatty acids[23] while lipid species were analyzed using a targeted multiple reaction monitoring (MRM) method[45]; MRM transitions are available in the *Metabolomics Workbench* repository.

RNA Extraction and RT-qPCR

The total RNA of 2D cells was collected from an equal number of intact cells in TRI Reagent (#TR118; Molecular Research Center). RNA was recovered after separation in 1-bromo-3-chloropropane and precipitation with isopropanol, washed with ethanol (70%), and resuspended in RNAse-free water. The total RNA of cells isolated from 3D spheroids after FACSorting was extracted using the Maxwell RSC SimplyRNA tissue kit (#AS1340; Promega) according to manufacturer's instructions including a DNAse treatment. RNA quantity and quality were evaluated with a Nanodrop 1000 spectrophotometer (Thermo Fisher Scientific). After reverse transcription on 500 ng of total RNA with the RevertAid Reverse-Transcriptase, oligo-dT, and random hexamers (Thermo Fisher Scientific), quantitative PCR amplification was performed on the CFX Connect Real-Time PCR detection system (#1855201, Biorad) using Takyon Low Rox SYBR® MasterMix dTTP Blue (#UFLSMT-B0701; Eurogentec) and sequence-specific primers for SCD (FW:TCATAATTCCCGACGTGGCT; REV:CCAGGTTTGTAGTACCTCCT CTG), SCD5 (FW:CATCTGGGGAGAGAGTCTGTG; REV:ATTATGGAAG CCTTCACCAATGGC), FADS1 (FW:TGCAATGTCCACAAGTCTGC; REV: AGCTGCCCTGACTCCTTTAG), and FADS2 (FW:GACCACGGCAAGAAC TCAAAG; REV:GAGGGTAGGAATCCAGCCATT) genes. Relative gene expression was calculated using the ddCt method, with RPLP0 (FW: AGCCCAGAACACTGGTCTC; REV: ACTCAGGATTTCAATGGTGCC) as the reference gene.

Western blotting

Cancer cells were washed with PBS and lysed in a RIPA buffer supplemented with a protease inhibitor. Protein concentration was determined using a bicinchoninic acid-based assay (Thermo Fisher Scientific). A sample denaturation was performed for 7 min at 95 °C with Laemmli sample buffer containing 100 mM dithiothreitol. Then, samples (25 mg per well) were separated by SDS-PAGE (15% acrylamide/bis-acrylamide gels) and transferred onto PVDF membranes. Membranes were then blocked with 5% skimmed milk diluted in TBS-0.1% Tween 20 (TTBS) and immunoblotted overnight at 4 °C with the specific SCD1 (#ab236868, Abcam, 1:1000), BiP (#3177, Cell Signaling Technology, 1:1000), ATF4 (#11815 Cell Signaling Technology, 1:1000) primary antibody and HSP90 (#610419, BD Biosciences, 1:10,000) or β-actin (A5441, Sigma-Merck, 1:10,000) primary antibody as housekeeping. After several washes with TTBS, membranes were incubated for 1 h at room temperature with horseradish peroxidase (HRP)-conjugated secondary antibodies (Jackson Immunoresearch), and chemiluminescent signals were revealed by using ECL Western Blotting Detection Kit (GE Healthcare) on X-ray films in a dark chamber.

IncuCyte experiments

The IncuCyte (#SX5, Sartorius) was used to assess spheroid growth and toxicity with the IncuCyte Cytotox Green Reagent (#4633, Sartorius, 25 nM) according to the manufacturer's recommendation. The Cytotox Green reagent was added to the culture together with inhibitors (7 days after spheroid formation). Spheroid images were acquired every 6 h with the 10× objective, the area, and the green fluorescence were measured with the Incucyte Software.

Seahorse experiments

All monolayer cells were plated in on Seahorse Bioanalyzer XFe96 culture plates overnight in DMEM media before treatment with SCD1i (15 μM), with or without palmitic acid or stearic acid (25 μM). Spheroids were treated in Ultra-Low attachment plates with SCD1i (15 μM) 24 h before being transferred to XFe96 Spheroid Microplates plates, precoated with poly-D lysine (50 μg/mL). For all experiments, cells were incubated for 45 min à 37 °C in Seahorse XF-base medium supplemented with 1 mM glucose and 1 mM glutamine, before the experiment. According to the test, pH was maintained at 7.4 or 6.5, with or without SCD1i (15 μM) and PA (25 μM). OCR was measured with Seahorse XFe96 Analyzer (Agilent) and data analysis was performed using Seahorse Wave 2.4 software.

Acidic-conditioned medium and hypoxic conditions

When acidic adapted cancer cells reached 60% confluence of a 6-well plate, FADU, and HCT116 were treated respectively with 15 μM or 25 μM SCDi, in 6.5 medium complemented with 5% of delipidated FBS (S181L-500, VWR), 50 μM PA and 10 μM OA, for 24H. Half of the medium volume was used to quantify FA, the other was used as a conditioned medium to treat acidic cancer cells in a hypoxia chamber at 1% O2, 5% CO_2, 37 °C (H35 Hypoxystation, Don Whitley Scientific). As a third, 50 μM OA was added in the control conditioned medium and as a fourth condition, SCDi was added in the control conditioned medium at the concentrations described above and a non-conditioned medium complemented as described above was used as control. After 48 h incubation, cell viability was determined by using the Presto blue reagent (A13261, Thermo Fisher Scientific) according to the manufacturer's instructions.

In vivo mouse experiments

All mice were housed in the same experimental room with the appropriate 12 h light/12 h dark cycles and controlled for temperature (21-24 °C) and humidity (40-60%). Mice were fed with isocaloric control (Safe, U8978 P0177) or PUFA-rich anchovy/sardine oil-containing (Safe, U8978 P0177) diet. Rj:NMRI-Foxn1nu/nu 5-week female mice (Janvier), were first accommodated to the specific diets for two weeks prior to cancer cell injection, the diets were maintained throughout the experiment. Before injection control or SCD1 knock out FaDu cancer cells were washed twice with PBS, resuspended in 0.9% NaCl and 2×10^6 cells were injected in the right flank of each mouse. When tumors reached 50–100 mm^3, mice were treated with SCD1 inhibitor (30 mg/kg) diluted in DMSO by intraperitoneal injection for 5 days per week for three weeks. Control groups were treated in parallel with equivalent vehicles. Mice were weighed once per week and tumors were measured 3 times a week. None of the tumor volumes of mice in this study exceeded the limits authorized by the local ethical committee. At the end of the experiment, when tumor size reached the ethical endpoint (500 mm^3 or

visible necrosis), mice were sacrificed and blood, liver, and tumors were collected. Collected samples were separated in two for fatty acid quantification, and immunohistochemistry.

Statistics and reproducibility

Statistical analyses were performed through GraphPad Prism 10 by using Student's *t*-test, one-way ANOVA with Tukey's, Sidak's or Dunnet's multiple comparison test, two-way ANOVA with Tukey's multiple comparison tests or with Fisher's LSD test and Long-rank Mantel–Cox test when appropriate. Statistical significance is indicated as follows: exact *P*-values are provided when $^{*}P \leq 0.05$ or $^{**}P < 0.01$, while $^{***}P < 0.001$ and $^{****}P < 0.0001$ indicate threshold values. No statistical method was used to predetermine the sample size. The experimental sample size was chosen based on commonly accepted standards. No data were excluded from the analyses. Mice were randomly assigned to each group, other experiments were not randomized. The investigators were not blinded to allocation during experiments and outcome assessment.

Reporting summary

Further information on research design is available in the Nature Portfolio Reporting Summary linked to this article.

Data availability

The dataset from RNA-sequencing analysis, generated during this study, is available at Gene Expression Omnibus GSE250335: https://www.ncbi.nlm.nih.gov/geo/query/acc.cgi?acc=GSE250335 The lipidomic raw data are *available at the NIH Common Fund's National Metabolomics Data Repository (NMDR) website, the Metabolomics Workbench*, https://www.metabolomicsworkbench.org *where it has been assigned Project ID PR002183. The data can be accessed directly* via *it's Project DOI:* https://doi.org/10.21228/M8FK0S. The RRID for the 2IP Imaging Platform is SCR_023378. Source data are provided with this paper.

References

1. Corbet, C. & Feron, O. Tumour acidosis: from the passenger to the driver's seat. *Nat. Rev. Cancer* **17**, 577–593 (2017).
2. Swietach, P., Boedtkjer, E. & Pedersen, S. F. How protons pave the way to aggressive cancers. *Nat. Rev. Cancer* **23**, 825–841 (2023).
3. Corbet, C. & Feron, O. Cancer cell metabolism and mitochondria: nutrient plasticity for TCA cycle fueling. *Biochim. Biophys. Acta Rev. Cancer* **1868**, 7–15 (2017).
4. Newell, K., Franchi, A., Pouyssegur, J. & Tannock, I. Studies with glycolysis-deficient cells suggest that production of lactic acid is not the only cause of tumor acidity. *Proc. Natl Acad. Sci. USA* **90**, 1127–1131 (1993).
5. Yamagata, M., Hasuda, K., Stamato, T. & Tannock, I. F. The contribution of lactic acid to acidification of tumours: studies of variant cells lacking lactate dehydrogenase. *Br. J. Cancer* **77**, 1726–1731 (1998).
6. Helmlinger, G., Sckell, A., Dellian, M., Forbes, N. S. & Jain, R. K. Acid production in glycolysis-impaired tumors provides new insights into tumor metabolism. *Clin. Cancer Res.* **8**, 1284–1291 (2002).
7. Mookerjee, S. A., Goncalves, R. L. S., Gerencser, A. A., Nicholls, D. G. & Brand, M. D. The contributions of respiration and glycolysis to extracellular acid production. *Biochim. Biophys. Acta* **1847**, 171–181 (2015).
8. Vaupel, P. W., Frinak, S. & Bicher, H. I. Heterogeneous oxygen partial pressure and pH distribution in C3H mouse mammary adenocarcinoma. *Cancer Res.* **41**, 2008–2013 (1981).
9. Helmlinger, G., Yuan, F., Dellian, M. & Jain, R. K. Interstitial pH and pO2 gradients in solid tumors in vivo: high-resolution measurements reveal a lack of correlation. *Nat. Med.* **3**, 177–182 (1997).
10. Corbet, C. et al. The SIRT1/HIF2alpha axis drives reductive glutamine metabolism under chronic acidosis and alters tumor response to therapy. *Cancer Res.* **74**, 5507–5519 (2014).
11. Corbet, C. et al. Acidosis drives the reprogramming of fatty acid metabolism in cancer cells through changes in mitochondrial and histone acetylation. *Cell Metab.* **24**, 311–323 (2016).
12. Michl, J. et al. CRISPR-Cas9 screen identifies oxidative phosphorylation as essential for cancer cell survival at low extracellular pH. *Cell Rep.* **38**, 110493 (2022).
13. Rolver, M. G. et al. Chronic acidosis rewires cancer cell metabolism through PPARalpha signaling. *Int J. Cancer* **152**, 1668–1684 (2023).
14. Yao, J. et al. Cancer cell acid adaptation gene expression response is correlated to tumor-specific tissue expression profiles and patient survival. *Cancers* **12**, 2183 (2020).
15. Corbet, C. et al. TGFbeta2-induced formation of lipid droplets supports acidosis-driven EMT and the metastatic spreading of cancer cells. *Nat. Commun.* **11**, 454 (2020).
16. Zhu, S. et al. ASIC1 and ASIC3 contribute to acidity-induced EMT of pancreatic cancer through activating Ca(2+)/RhoA pathway. *Cell Death Dis.* **8**, e2806 (2017).
17. Cui, J. et al. Carbonic anhydrase IX inhibitor S4 triggers release of DAMPs related to immunogenic cell death in glioma cells via endoplasmic reticulum stress pathway. *Cell Commun. Signal* **21**, 167 (2023).
18. Swietach, P., Hulikova, A., Vaughan-Jones, R. D. & Harris, A. L. New insights into the physiological role of carbonic anhydrase IX in tumour pH regulation. *Oncogene* **29**, 6509–6521 (2010).
19. Swietach, P., Patiar, S., Supuran, C. T., Harris, A. L. & Vaughan-Jones, R. D. The role of carbonic anhydrase 9 in regulating extracellular and intracellular ph in three-dimensional tumor cell growths. *J. Biol. Chem.* **284**, 20299–20310 (2009).
20. Le, Q. T. et al. Expression and prognostic significance of a panel of tissue hypoxia markers in head-and-neck squamous cell carcinomas. *Int J. Radiat. Oncol. Biol. Phys.* **69**, 167–175 (2007).
21. Rademakers, S. E., Lok, J., van der Kogel, A. J., Bussink, J. & Kaanders, J. H. Metabolic markers in relation to hypoxia; staining patterns and colocalization of pimonidazole, HIF-1alpha, CAIX, LDH-5, GLUT-1, MCT1 and MCT4. *BMC Cancer* **11**, 167 (2011).
22. Bittner, M. I. et al. Analysis of relation between hypoxia PET imaging and tissue-based biomarkers during head and neck radiochemotherapy. *Acta Oncol.* **55**, 1299–1304 (2016).
23. Dierge, E. et al. Peroxidation of n-3 and n-6 polyunsaturated fatty acids in the acidic tumor environment leads to ferroptosis-mediated anticancer effects. *Cell Metab.* **33**, 1701–1715.e1705 (2021).
24. Magtanong, L. et al. Exogenous monounsaturated fatty acids promote a ferroptosis-resistant cell state. *Cell Chem. Biol.* **26**, 420–432.e429 (2019).
25. Ubellacker, J. M. et al. Lymph protects metastasizing melanoma cells from ferroptosis. *Nature* **585**, 113–118 (2020).
26. Kamphorst, J. J. et al. Hypoxic and Ras-transformed cells support growth by scavenging unsaturated fatty acids from lysophospholipids. *Proc. Natl Acad. Sci. USA* **110**, 8882–8887 (2013).
27. Piccolis, M. et al. Probing the global cellular responses to lipotoxicity caused by saturated fatty acids. *Mol. Cell* **74**, 32–44.e38 (2019).
28. Pastorekova, S. & Gillies, R. J. The role of carbonic anhydrase IX in cancer development: links to hypoxia, acidosis, and beyond. *Cancer Metastasis Rev.* **38**, 65–77 (2019).
29. Hofacer, R. et al. Omega-3 fatty acid deficiency increases stearoyl-CoA desaturase expression and activity indices in rat liver: positive association with non-fasting plasma triglyceride levels. *Prostaglandins Leukot. Essent. Fat. Acids* **86**, 71–77 (2012).
30. Bene, H., Lasky, D. & Ntambi, J. M. Cloning and characterization of the human stearoyl-CoA desaturase gene promoter: transcriptional activation by sterol regulatory element binding protein and

repression by polyunsaturated fatty acids and cholesterol. *Biochem. Biophys. Res. Commun.* **284**, 1194–1198 (2001).
31. Miller, C. W. & Ntambi, J. M. Peroxisome proliferators induce mouse liver stearoyl-CoA desaturase 1 gene expression. *Proc. Natl Acad. Sci. USA* **93**, 9443–9448 (1996).
32. Kondo, A. et al. Extracellular acidic pH activates the sterol regulatory element-binding protein 2 to promote tumor progression. *Cell Rep.* **18**, 2228–2242 (2017).
33. Peck, B. et al. Inhibition of fatty acid desaturation is detrimental to cancer cell survival in metabolically compromised environments. *Cancer Metab.* **4**, 6 (2016).
34. Savino, A. M. et al. Metabolic adaptation of acute lymphoblastic leukemia to the central nervous system microenvironment is dependent on Stearoyl CoA desaturase. *Nat. Cancer* **1**, 998–1009 (2020).
35. Lien, E. C. et al. Low glycaemic diets alter lipid metabolism to influence tumour growth. *Nature* **599**, 302–307 (2021).
36. Young, R. M. et al. Dysregulated mTORC1 renders cells critically dependent on desaturated lipids for survival under tumor-like stress. *Genes Dev.* **27**, 1115–1131 (2013).
37. Ackerman, D. et al. Triglycerides promote lipid homeostasis during hypoxic stress by balancing fatty acid saturation. *Cell Rep.* **24**, 2596–2605.e2595 (2018).
38. Ma, M. K. F. et al. Stearoyl-CoA desaturase regulates sorafenib resistance via modulation of ER stress-induced differentiation. *J. Hepatol.* **67**, 979–990 (2017).
39. Listenberger, L. L. et al. Triglyceride accumulation protects against fatty acid-induced lipotoxicity. *Proc. Natl Acad. Sci. USA* **100**, 3077–3082 (2003).
40. Griffiths, B. et al. Sterol regulatory element binding protein-dependent regulation of lipid synthesis supports cell survival and tumor growth. *Cancer Metab.* **1**, 3 (2013).
41. Tesfay, L. et al. Stearoyl-CoA desaturase 1 protects ovarian cancer cells from ferroptotic cell death. *Cancer Res.* **79**, 5355–5366 (2019).
42. Friedmann Angeli, J. P., Krysko, D. V. & Conrad, M. Ferroptosis at the crossroads of cancer-acquired drug resistance and immune evasion. *Nat. Rev. Cancer* **19**, 405–414 (2019).
43. Man, W. C., Miyazaki, M., Chu, K. & Ntambi, J. Colocalization of SCD1 and DGAT2: implying preference for endogenous monounsaturated fatty acids in triglyceride synthesis. *J. Lipid Res.* **47**, 1928–1939 (2006).
44. Susaki, E. A. et al. Advanced CUBIC protocols for whole-brain and whole-body clearing and imaging. *Nat. Protoc.* **10**, 1709–1727 (2003).
45. Nassar, Z. D. et al. Human DECR1 is an androgen-repressed survival factor that regulates PUFA oxidation to protect prostate tumor cells from ferroptosis. *eLlife* **9**, e54166 (2020).

Acknowledgements

This work was supported by grants from the Fonds de la Recherche Scientifique (F.R.S.-FNRS, PDR T008719F and EOS O002522F), WELBIO (Walloon Excellence in Life Sciences and Biotechnology, X104022F), the (Belgian) Foundation against cancer (2020-074), and an Action de Recherche Concertée (ARC 19/24-096). C.C. is an F.R.S.-FNRS Research Associate and a Walloon Excellence in Life Sciences and Biotechnology (WELBIO) junior fellow. O.F. is a senior WELBIO investigator.

Author contributions

Conceptualization: O.F., K.G., and S.I.; experimental work: K.G., S.I., O.R., P.V., M.V.G., K.O., C.G., and F.L.M.; data analysis and interpretation: O.F., K.G., S.I., J.A.; methodology: C.D., L.A., C.B., D.B., E.R., J.D., and J.S.; Writing: O.F., K.G., S.I., and O.R..; Funding: O.F.; Resources: O.F., C.C., and Y.L.; Supervision: O.F.

Competing interests

The authors declare no competing interests.

Additional information

Supplementary information The online version contains supplementary material available at https://doi.org/10.1038/s41467-024-54435-3.

Correspondence and requests for materials should be addressed to Olivier Feron.

Peer review information *Nature Communications* thanks Pawel Swietach, and the other, anonymous, reviewer(s) for their contribution to the peer review of this work. A peer review file is available.